Title: Atomistic Conversion Reaction Mechanism of WO3 in Secondary Ion Batteries of Li, Na, and Ca

Authors: Chongmin Wang; Yang He; Meng Gu; Haiyan Xiao; Langli Luo; Yuyan Shao; Fei Gao; Yingge Du; Scott Mao

To be cited as: 10.1002/anie.201601542

Link to VoR: http://dx.doi.org/10.1002/anie.201601542

Atomistic Conversion Reaction Mechanism of WO_3 in Secondary Ion Batteries of Li, Na, and Ca

Yang He[2†], Meng Gu[1†], Haiyan Xiao[3], Langli Luo[1], Yuyan Shao[4], Fei Gao[5*], Yingge Du[1*], Scott X. Mao[2*] and Chongmin Wang[1*]

[1]Environmental Molecular Sciences Laboratory, Pacific Northwest National Laboratory, Richland, Washington, 99352, USA
[2]Department of Mechanical Engineering and Materials Science, University of Pittsburgh, Pittsburgh, Pennsylvania, 15261, USA
[3]School of Physical Electronics, University of Electronic Science and Technology of China, Chengdu, 610054, China
[4]Energy and Environmental Directorate, Pacific Northwest National Laboratory, Richland, Washington, 99352, USA
[5]Department of Nuclear Engineering and Radiological Sciences, University of Michigan, Ann Arbor, Michigan, 48109,

Supporting Information is available for this article.

ABSTRACT: Intercalation and conversion are two fundamental chemical processes for battery materials in response to ion insertion. The interplay between these two chemical processes has never been directly seen and understood at atomic scale. Here, using *in-situ* HRTEM, we captured the atomistic conversion reaction processes during Li, Na, Ca insertion into WO_3 single crystal model electrodes. An intercalation step right prior to conversion is explicitly revealed at atomic scale for the first time for Li and Ca. Nanoscale diffraction and *ab initio* molecular dynamics simulations found that, going beyond intercalation, the inserted ion-oxygen bonding formation destabilized the transition-metal framework which gradually shrunk, distorted and finally collapsed to amorphous W and M_xO(M=Li,Na,Ca) composite structure. This study provides a full atomistic picture on the transition from intercalation to conversion, which is of essential importance for both secondary ion batteries and electrochromic devices.

Conversion-type lithium ion batteries (LIB) using electrodes such as transition metal oxides, hydrides, and sulfides are capable of utilizing all possible oxidation states of a compound, and thus can provide large specific capacity for advanced applications such as electrical vehicles.[1] Understanding the atomistic conversion mechanism is fundamentally important in searching for new conversion-type electrode materials and the application of these materials.[2] Unfortunately, the conversion mechanism has not been explicitly established mostly because the process is wrapped in a nanoscale narrow reaction front. By atomistic simulations and detecting traces of intermediate phase, it is proposed that the conversion process is likely initiated by ion intercalation into the electrode materials, e.g. FeF_2,[2d] SnO_2,[3] Co_3O_4,[4] Fe_2O_3,[5] RuO_2,[6] MoO_3[7] and WO_3.[8] However, the methods including X-ray diffraction and selected area electron diffraction from a broad area across the reaction front are too ensemble-averaged to clearly resolve the relation between the intercalation and conversion. Besides, how the crystalline intercalation phase evolves to fully-charged conversion phases lacks detailed experimental investigation at the atomic scale. Here, using nano-beam diffraction (NBD) and electron energy loss spectroscopy (EELS) coupling with scanning/transmission electron microscopy (S/TEM), we investigated the structural and chemical evolution across a conversion reaction front with high spatial resolution in WO_3 upon electrochemical ions (Li, Na, Ca) insertion.

WO_3 is an ideal model system to study the intercalation initiated conversion reaction, and the interplay between these two chemical processes. It is a widely studied electrochromic material as its pseudo-cubic cell contains a large, empty center site, providing an open environment for small ion (e.g., H and Li) reversible intercalation/removal. Due to the same reason and the high valance state that can theoretically host maximum 6 alkali metal ions or 3 alkaline earth metal ions,[7, 9] WO_3 has also recently received interest as candidate of conversion-type anode for next generation multivalent ion batteries.[10]

The test setup is shown in Figure 1a. Single crystalline WO_3 films grown epitaxially on conductive Nb-doped $SrTiO_3$(001) (Nb-STO) substrate by molecular beam epitaxy was used as electrodes in a half solid-cell setup. Details on film growth and characterization have been published elsewhere.[11] Electron diffraction (inset in Figure 1c) indicates that as-grown WO_3 has a monoclinic structure (space group P 21/c), which is in good agreement with WO_3 used in LIB.[9b] The hetero-epitaxial architecture provides high mechanical stability for high resolution TEM imaging and guarantees good electrical contact through conductive Nb-STO. Pure metals of Li, Na, and Ca were used as ion sources. The surface oxides due to short time air-exposure, i.e. Li_2O, Na_2O, and CaO, worked as electrolytes for ions. The ion source is manipulated by piezo-system to contact the WO_3 electrode at one end, and then biased (-0.8V) with respect to the WO_3 film to drive the electrochemical reaction.

General morphology evolution of WO_3 during Li^+ insertion is shown by the sequential bright field TEM images in Figure 1c. The reaction front (white dash line in Figure 1c) is roughly perpendicular to WO_3 [001] direction, implying that Li atoms diffused along [010] lattice channel. This claim is supported by the atomic resolution images in Figure 1d which shows a reaction front penetrating along ⟨001⟩ into the lattice. Different from many other electrode materials,[3b, 12] there was no high density dislocations, or "Medusa" zone, at the propagating reaction front (Supporting Movie 1), which can be attributed to the small volume expansion as a result of the spacious lattice channels (3.8 Å) for ion conduction in WO_3. Assuming equal expansion along three

⟨001⟩ directions, the volume expansion at full lithiation was estimated to be ~17%, which was much lower than SnO_2[12] or Si (~300%).[13] After fully charged with Li, the crystalline WO_3 was converted to amorphous W (a-W) metal and Li_2O as indicated by the electron diffraction pattern (inset in Figure 1c). The electron beam effect is described in detail in Supporting Information.

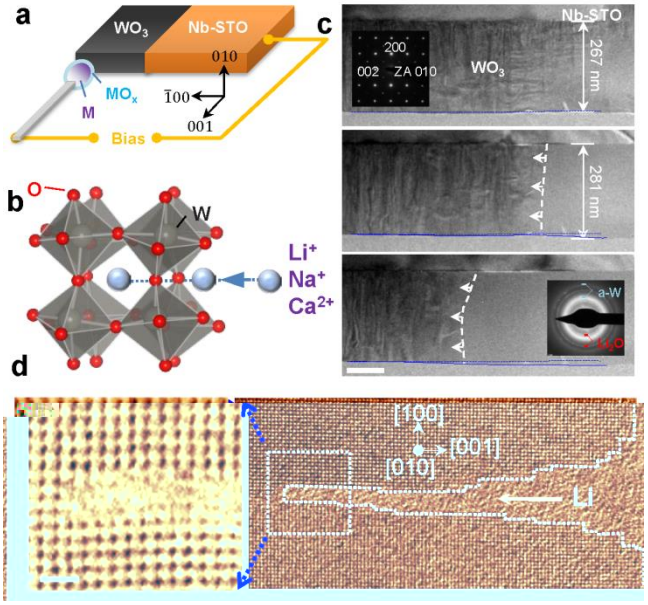

Figure 1. a) Schematics of the *in situ* experiment setup, (M=Li, Na, Ca) b) Atomic structural model of monoclinic WO_3 showing WO_6 octahedral and vacant site with Li (Na, or Ca) transporting along the channel into the vacant A site, c) Sequential TEM bright field images showing WO_3 structure evolution during Li insertion (lithiation). Insets show electron diffraction patterns of pristine and fully lithiated phases. White dash lines mark reaction front. Cyan lines mark surface position highlighting the volume expansion. Scale bar, 100 nm. d) High resolution TEM image of a local region on the reaction front (dash line). Inset on left is an atomic resolution annular dark field image of the boxed region. Scale bar, 1 nm.

To reveal the reaction mechanism, Li_xWO_3 phase and W valance state evolution across the reaction front were analyzed with NBD and EELS line scan (Figure 2, S2, and S3 and Supporting Movie 2). On the right side of the reaction front (e.g. position 3 and 4 in Figure 2a), diffused amorphous ring appeared in the NBDs, meaning that the structure lost crystallinity beyond the reaction front (CF). Surprisingly, near the left side of the CF, the NBD shows significant variations compared to the pristine WO_3, even though the crystallinity is well preserved.

Measurement from NBD shows that, approaching from far left to CF, the d-spacing of (002) planes slightly decreased. More obviously, at position 2 in Figure 2, some diffraction spots disappeared compared to that of pristine WO_3. Referring to known structures of Li_xWO_3,[8a] this change is consistent with gradual Li concentration increase from left to right. At position 2, the concentration reached a maximum Li intercalation value with crystalline symmetry changing from the original P21/c monoclinic structure to the final intercalated cubic phase, which is also consistent with the detailed phase diagram measured by in-situ XRD measurement.[8a, 14] However, the critical maximum Li concentration that can be intercalated into WO_3 may depend critically on the dimensionality, size, and structural stability of the specific WO_3 materials. As reported by Qiang et al,[14] the WO_3 nanorods with a high aspect ratio yield an intercalation capacity of 1.12 Li per formula unit, which is much higher than 0.5 Li per formula unit for bulk WO_3 powder as reported by Zhong et al.[8a] The maximum value of Li concentration in the final cubic phase need further evaluation using light-element-sensitive method such as atom probe tomography.[15] In addition, scanning from left to right of CF, spatial-resolved EELS spectrums (Supporting Figure S2) show that the intensity of Li *K*-edge gradually increased and the O_2-edge of W monotonically shifted from 56.5 eV to 54.5 eV, indicating W valance state decrease with Li^+ insertion.[2b] These structure and spectroscopy information explicitly proves that Li intercalated into the WO_3 before conversion reaction, and the lithium concentration gradually increased in the intercalation region until conversion started at the CF. The structure evolution is vividly illustrated by schematic models in Figure 2c. The intercalation front (IF) cannot be accurately determined (dash line in Figure 2a), because, at very low *x* values (going farther beyond the CF), Li_xWO_3 has very similar NBD pattern with pristine WO_3 and has trivial volume change and weak Li *K*-edge signal in the EELS spectrum. However, the distance between the CF and the point where cubic diffraction pattern is obtained (Figure 2 point 3) is ~60 nm, meaning that the thickness of intercalation region should be at least 60 nm.

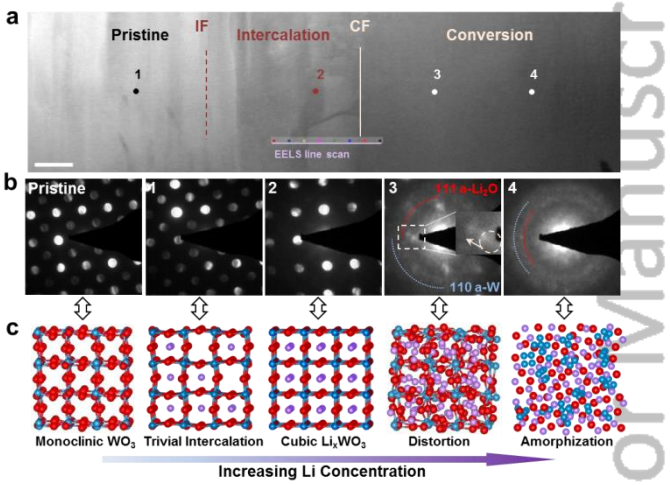

Figure 2. a) High angle annular dark field (HAADF) scanning transmission electron microscopy (STEM) image of the reaction front in Figure 1c. Scale bar, 50 nm. b) Nano beam diffractions (NBD) from the pristine sample and across the conversion front (CF), c) Schematics of the structure and crystal symmetry evolution with increasing Li concentration in the Li_xWO_3 lattice as indicated by the corresponding NBDs.

With increasing Li concentration, the intercalation phase gradually transformed to amorphous starting from the CF. As shown in Supporting Figure S3a, the NBD spots of intercalation phase continuously shifted outward both tangentially and radially as shown by the red arrows. The lattice was cubic after intercalation as shown by the red square pattern of the diffraction spot. However, after further insertion of Li ions, the lattice distorted and the diffraction pattern of the original red square changed to irregular shape and finally a diffraction ring pattern appears. *Ab* initio molecular dynamics simulations (Supporting Figure S3b-c) consistently indicate the excessive Li ions bonded with O atoms and distorted of WO_3 framework towards the formation of Li_2O and W metal ordering. A detailed analysis on the intercalation to conversion transition is provided in supporting information.

Similar to the case of Li^+ insertion, with continuous Na^+ insertion, the CF progressively propagated upward from the bottom contact

with Na source (Supporting Movie 3). Figure 3b shows a HRTEM snapshot of the CF. Fast Fourier transformations (FFT) of the local regions in the image (insets in Figure 3b) were used to analyze the phases across the CF. The FFT of the region right above the CF can only be assigned to cubic Na_xWO_3 with aligned WO6 octahedral. The FFT of the converted region shows the formation of W nanocrystals. These phases can also be identified from the select area diffraction (SAD) patterns in Figure 3d taken from the circled region in Figure 3a; besides the diffraction rings from the W metal and $Na_2$of W

Department of Energy (DOE) under Contract DE-AC05-76RL01830. The research was performed using the Environmental Molecular Sciences Laboratory (EMSL), a national scientific user facility sponsored by the Department of Energy's Office of Biological and Environmental Research and located at PNNL.

Keywords: intercalation · conversion · lithium ion batteries · *in situ* TEM · WO_3

[1] P. Poizot, S. Laruelle, S. Grugeon, L. Dupont, J.-M. Tarascon, *Nature* **2000**, *407*, 496-499.

[2] aSung-Wook Kim, Nathalie Pereira, Natasha A Chernova, Fredrick Omenya, Peng Gao, M Stanley Whittingham, Glenn G Amatucci, Dong Su, Feng Wang, *ACS Nano* **2015**, *9*, 10076-10084; bM. Langell, S. Bernasek, *Physical Review B* **1981**, *23*, 1584-1593; cKai He, Feng Lin, Yizhou Zhu, Xiqian Yu, Jing Li, Ruoqian Lin, Dennis Nordlund, Tsu-Chien Weng, Ryan M Richards, Xiao-Qing Yang, Marca M Doeff, Eric A Stach, Yifei Mo, Huolin L Xin, D. Su, *Nano Lett.* **2015**, *15*, 5755-5763; dF. Wang, H. C. Yu, M. H. Chen, L. Wu, N. Pereira, K. Thornton, A. Van der Ven, Y. Zhu, G. G. Amatucci, J. Graetz, *Nature communications* **2012**, *3*, 1201; eKai He, Yongning Zhou, Peng Gao, Liping Wang, Nathalie Pereira, Glenn G Amatucci, Kyung-Wan Nam, Xiao-Qing Yang, Yimei Zhu, Feng Wang, D. Su, *ACS Nano* **2014**, *8*, 7251-7259.

[3] aA. Nie, L. Y. Gan, Y. Cheng, H. Asayesh-Ardakani, Q. Q. Li, C. Z. Dong, R. Z. Tao, F. Mashayek, H. T. Wang, U. S. Schlogl, R. F. Kile, R. S. Yassar, *ACS Nano* **2013**, *7*, 6203-6211; bL. Zhong, X. H. Liu, G. F. Wang, S. X. Mao, J. Y. Huang, *Physical Review Letters* **2011**, *106*, 248302.

[4] L. Luo, J. Wu, J. Xu, V. P. Dravid, *ACS Nano* **2014**, *8*, 11560-11566.

[5] Q. Su, D. Xie, J. Zhang, G. Du, B. Xu, *ACS Nano* **2013**, *7*, 9115-9121.

[6] K. E. Gregorczyk, Y. Liu, J. P. Sullivan, G. W. Rubloff, *ACS Nano* **2013**, *7*, 6354-6360.

[7] L. Q. Mai, B. Hu, W. Chen, Y. Y. Qi, C. S. Lao, R. S. Yang, Y. Dai, Z. L. Wang, *Advanced Materials* **2007**, *19*, 3712-3716.

[8] aQ. Zhong, J. Dahn, K. Colbow, *Physical Review B* **1992**, *46*, 2554-2560; bS. H. Lee, M. J. Seong, H. M. Cheong, E. Ozkan, E. C. Tracy, S. K. Deb, *Solid State Ionics* **2003**, *156*, 447-452; cK. Qi, J. Wei, M. Sun, Q. Huang, X. Li, Z. Xu, W. Wang, X. Bai, *Angew Chem Int Ed Engl* **2015**, *54*, 15222-15225.

[9] aS. H. Lee, Y. H. Kim, R. Deshpande, P. A. Parilla, E. Whitney, D. T. Gillaspie, K. M. Jones, A. H. Mahan, S. Zhang, A. C. Dillon, *Advanced Materials* **2008**, *20*, 3627-3632; bW. J. Li, Z. W. Fu, *Applied Surface Science* **2010**, *256*, 2447-2452.

[10] H. Yuan, L. Jiao, J. Cao, X. Liu, M. Zhao, Y. Wang, *J. Mater. Sci. Technol.* **2004**, *20*, 41-45.

[11] Y. Du, M. Gu, T. Varga, C. Wang, M. E. Bowden, S. A. Chambers, *ACS Applied Materials & Interfaces* **2014**, *6*, 14253-14258.

[12] J. Y. Huang, L. Zhong, C. M. Wang, J. P. Sullivan, W. Xu, L. Q. Zhang, S. X. Mao, N. S. Hudak, X. H. Liu, A. Subramanian, H. Fan, L. Qi, A. Kushima, J. Li, *Science* **2010**, *330*, 1515-1520.

[13] Y. He, D. M. Piper, M. Gu, J. J. Travis, S. M. George, S. H. Lee, A. Genc, L. Pullan, J. Liu, S. X. Mao, J. G. Zhang, C. Ban, C. Wang, *ACS Nano* **2014**, *8*, 11816-11823.

[14] W. Qiang, W. Zhenhai, J. Yeonseok, C. Jiyoung, L. Kwangyeol, L. Jinghong, *Nanotechnology* **2006**, *17*, 3116.

[15] A. Devaraj, M. Gu, R. Colby, P. Yan, C. M. Wang, J. M. Zheng, J. Xiao, A. Genc, J. G. Zhang, I. Belharouak, D. Wang, K. Amine, S. Thevuthasan, *Nature communications* **2015**, *6*.

[16] A. Ponrouch, C. Frontera, F. Barde, M. R. Palacin, *Nature Materials* **2015**, *1*, 1-5.

TOC graphic